J Mater Sci (2012) 47:4036–4041
DOI 10.1007/s10853-012-6257-x

Interfacial reactions between Sn–57Bi–1Ag solder and electroless Ni-P/immersion Au under solid-state aging

Christopher Fuchs · Timo Schreck · Michael Kaloudis

Received: 17 October 2011 / Accepted: 5 January 2012 / Published online: 14 January 2012
© Springer Science+Business Media, LLC 2012

Abstract Interfacial reactions between Sn–57Bi–1Ag and electroless Ni-P/immersion Au were investigated following isothermal aging at 85 and 130 °C. A long-term aging study confirmed two intermetallics at the solder/substrate interface. With scanning electron microscopy and energy-dispersive X-ray spectroscopy (EDX) analysis, the metastable $NiSn_4$ phase was detected coexisting with the stable Ni_3Sn_4 phase. The average thicknesses of both intermetallic compounds (IMCs) were graphically plotted versus the square root of aging time. The EDX showed that Ni_3Sn_4 nucleated first. However, after nucleation, the IMC of the $NiSn_4$ phase grew faster than the one of Ni_3Sn_4 between 85 and 130 °C. For both temperatures, the growth constants were calculated and the corresponding activation energies were approximated. A high volume of Kirkendall voids appeared along the Ni_3Sn_4/$NiSn_4$ interface at 130 °C, resulting in dramatic shear strength decline.

Introduction

The Sn–Bi system is a simple binary system without any intermetallic compounds (IMCs), similar to the eutectic Sn–Pb system [1]. Due to their low melting point of 138 °C, solder alloys on Sn–58Bi basis are suitable lead-free candidates for heat-sensitive materials and devices. Their price and mechanical properties, such as elastic modulus and tensile strength, are also comparable to those of the Sn–40Pb alloy [2]. Although the microstructure of Sn–58Bi has a lower ductility than the one of Sn–Pb [3], it can be improved by the use of adding elements, for example, silver (Ag) [4]. Since Ag improves the plasticity of the eutectic Sn–58Bi solder, Sn–57Bi–1Ag is a solder alloy that is preferentially used. Its total elongation properties can be increased by 20% under the same processing conditions adding 0.5–1 wt% Ag, without any noticeable increase of the melting point [5]. Also, Dong et al. [6] showed that small amounts of 0.5 wt% Ag as well as rare earth elements can refine the microstructure to improve the shear strength of solder joints for both after as-reflowed condition and after thermal aging at 80 °C.

During the soldering process, solder alloys interact both physically and chemically with the substrate material [7]. After the flux has activated the solder/substrate interface, the molten solder wets the substrate surface, dissolves the substrate material to form IMCs by diffusing active constituent elements of both materials [8]. IMCs between solder/substrate interfaces are crucial to guarantee a mechanical and electrical interconnect. However, the interaction of the alloy with Cu or electroless Ni-P/Au substrate materials can cause complex interfacial reactions. Both the microstructure and the mechanical properties of the solder joints can be affected. Considering that solder/substrate interactions can have a significant impact on the performance of electronic applications, it is important to be aware of the intermetallic structure [9].

IMCs are generally brittle. Hence, their growth during usage affects the maximum shear load of the solder joints. The interfacial reactions of the Sn–58Bi/Cu couple after reflow and solid-state aging at various temperatures and their influence on the interconnection was fundamentally investigated [10–12]. Since IMC growth between Sn and Ni interfaces is slow, Sn–58Bi/Ni is another interesting

C. Fuchs · T. Schreck · M. Kaloudis (✉)
Laboratory for Packaging and Integrated Circuits, University of Applied Sciences, Aschaffenburg, Wuerzburger Str. 45, 63743 Aschaffenburg, Germany
e-mail: michael.kaloudis@h-ab.de
URL: www.h-ab.de

lead-free solder/substrate combination. A commonly used substrate finish is electroless Ni-P/immersion Au (ENIG). The advantage of these finishes is that they can be produced very flat, which makes them perfect for fine lead-pitch and area-array surface mount components [13]. The immersion Au layer (0.02–0.2 μm) prevents the Ni from being oxidized. It dissolves very fast into the solder during the reflow process. Some researchers studied the interfacial reaction Sn–58Bi/Ni after reflow and solid-state aging [13, 14] and molten state aging [15, 16]. According to the binary phase diagram Ni–Sn, three phases can exist at Sn/Ni interfaces—Ni_3Sn, Ni_3Sn_2, and Ni_3Sn_4. In some studies [13, 14], only Ni_3Sn_4 was found in Sn–Bi/Ni couples after various annealing times, while Ni_3Sn, Ni_3Sn_2, and $NiBi_3$ were merely found at temperatures higher than the melting point.

These thermodynamically stable phases with their particular composition and temperature are listed in a ternary phase diagram Sn–Bi–Ni [16]. However, phase diagrams do not normally comprise metastable phases which are not present after soldering [8]. Haimovich [17] found a plate-shaped metastable $NiSn_3$ phase. Similar to these phases, Chen and Chen [18] also found a Sn-rich metastable $NiSn_3$ phase coexisting with Ni_3Sn_4 formed in the Sn/Ni reaction zone at 100 °C. However, no other stable phases were found. They reported that Ni_3Sn_4 started forming, after $NiSn_3$ nucleated at the Ni_3Sn_4 grain boundaries, and then grew along the upper grain boundaries, nearly perpendicularly to the interface. Similarly to Haimovich's [17] plate-shaped phase, Boettinger et al. [19] reported a metastable $NiSn_4$ phase at the Ni/Sn reaction zone of their samples stressed with 1,500 thermocycles −40 °C/+130 °C. In their study, the $NiSn_4$ phase coexisted with Ni_3Sn_4 in the microstructure. Chuang et al. [20] also found metastable $NiSn_4$ whiskers at the Sn/Ni and SnAg/Ni interfaces at 150 °C. However, his metastable $NiSn_4$ phases were no longer observed with increasing aging time.

In this article, the interfacial IMC growth after solid-state aging at 85 and 130 °C with a Sn–57Bi–1Ag solder alloy on electroless Ni-P/Au substrate is discussed. The intermetallics at the solder/substrate interface and inside the microstructure were determined by energy-dispersive X-ray (EDX) analysis and discussed in comparison to the results found by some authors.

Experimental procedures

Sample preparation

A commercially available solder paste Sn–57Bi–1Ag from W.C. Heraeus and an ENIG substrate were used to prepare the samples for analysis. The Sn–57Bi–1Ag solder paste was printed on the ENIG substrate and soldered in a reflow oven under air atmosphere. Previously, a suitable reflow profile was defined to form the Sn–57Bi–1Ag/ENIG couples and the sandwiched ENIG/Sn–57Bi–1Ag/ENIG couples. All samples were soldered for 70 s at a temperature beyond 140 °C with its peak at 177 °C. For determination of the IMC growth, the solder/substrate interfaces were examined after reflow and after thermal aging at 85 and 130 °C for 800 and 200 h, respectively. To determine the influence of high temperature annealing on the shear strength of the solder joint, the ENIG/Sn–57Bi–1Ag/ENIG couples were stored at 130 °C. For this purpose, the diffusion couples were stored in an air furnace. The corresponding shear strength was measured after each annealing period. For examination, the samples were prepared metallographically.

Sample analysis

Scanning electron microscope (SEM) images were used for both to explore the interface and to measure the thickness of each IMC at the interface. The Olympus analysis software 'analysis docu' was used to determine the area of the interfacial IMCs for average thickness calculation. Four measurements of each specimen were taken to calculate a mean thickness value and an error term of ±standard deviation. The composition of the IMC was determined by EDX analysis.

Results and discussion

The microstructure of the Sn–57Bi–1Ag solder on ENIG substrate after reflow is shown in Fig. 1. At the eutectic temperature, Bi had significant solubility in Sn. Consequently, Bi participated in the Sn phase when the alloy cooled down [21]. As EDX analysis shows that the light region in the microstructure represents almost pure Bi. After using a Nital etching process, the Sn that was partly removed is displayed by the darker region inside the bulk solder. The SEM images show the intermetallic phases. A continuous thin layer grows along the Sn–57Bi–1Ag/ENIG interface. With EDX analysis, a composition of $Ni_{41at.\%}Sn_{50at.\%}Au_{4at.\%}Bi_{5at.\%}$ was detected which is very close to the stable Ni_3Sn_4 phase with small amounts of Au and Bi substituting for Sn. IMC growth measurements showed a very thin average layer thickness of approximately 0.1 μm. On the Ni_3Sn_4 interface, a needle-shaped second interfacial intermetallic with the stoichiometry of $Ni_{18at.\%}Sn_{70at.\%}Bi_{8at.\%}Au_{4at.\%}$ was localized. This phase composition suits very well to the previously discussed metastable $NiSn_4$ phase. Another intermetallic $Ag_{70at.\%}Sn_{25at.\%}Bi_{5at.\%}$ was found distributed in the bulk,

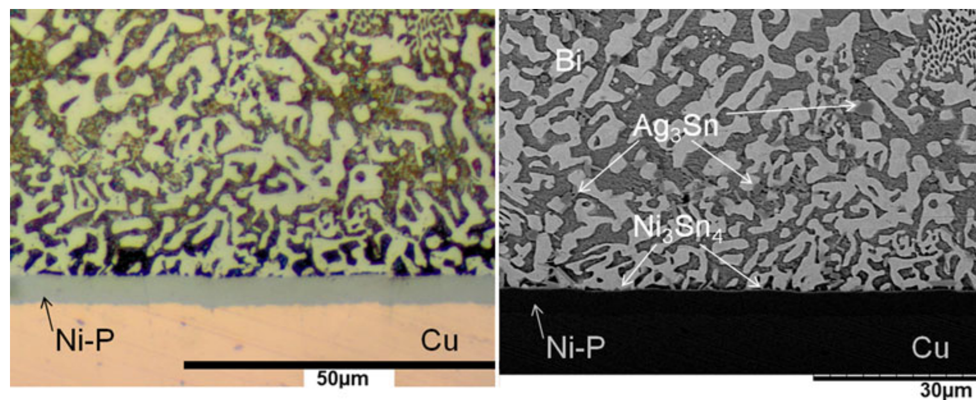

Fig. 1 Optical and SEM of the microstructure of Sn–57Bi–1Ag on ENIG

which represents the Ag_3Sn phase. In all phases, small amounts of Bi were also identified, whereas intermetallics with Au were detected at the interface.

Figure 2 shows the optical and the SEM image of the solder/substrate interface aged at 85 °C for 800 h. Similar to the initial microstructure, on the Ni-P layer, Ni_3Sn_4 with the exact stoichiometry of $Ni_{41at.\%}Sn_{55at.\%}Bi_{4at.\%}$ and $NiSn_4$ ($Ni_{16at.\%}Sn_{64at.\%}Bi_{10at.\%}Au_{10at.\%}$) were indentified, coexisting at the interface. In both scans, trace amounts of Bi are found in the IMC, while Au was demonstrably detected in the $NiSn_4$ phase. Both phases grew rather slowly, reaching a layer thickness of 0.5 and 0.9 µm, respectively, after 800 h of aging time. In the bulk solder, Ag_3Sn ($Ag_{73at.\%}Sn_{23at.\%}Bi_{4at.\%}$) intermetallics with small amounts of Bi were identified too.

Isothermal aging at 130 °C produced a fast growing $NiSn_4$ phase with whiskers up to 30 µm along the Ni_3Sn_4 interface, as displayed in Fig. 3. Its corresponding stoichiometric composition is $Ni_{15at.\%}Sn_{72at.\%}Bi_{13at.\%}$. In this phase, Au could hardly be detected anymore. While the average layer thickness of the Ni_3Sn_4 phase reached 1.4 µm, the $NiSn_4$ phase increased much faster to 3.3 µm. At the bottom of the $NiSn_4$ layer, voids appeared along the $Ni_3Sn_4/NiSn_4$ interface. On the ENIG pad, at the Ni-P/Ni_3Sn_4 interface, a Ni_3P phase was located. Along that Ni_3P layer cracks appeared. Further results from the EDX analysis detected another IMC between the Ni_3Sn_4 and Cu within the Ni-P layer. Its stoichiometry of $Ni_{49at.\%}Sn_{33at.\%}Bi_{6at.\%}Cu_{12at.\%}$ is very close to that of the stable Ni_3Sn_2 phase with amounts of Bi and Cu.

Due to the presence of Ag in the base alloy, the IMC Ag_3Sn could be found distributed within the microstructure just like Kattner and Boettinger [22] had described the ternary phase diagram Sn–Bi–Ag before. The coexistence of Ni_3Sn_4 and the metastable $NiSn_3$—or $NiSn_4$ in this study—after thermal aging at 85 and 130 °C was previously discussed by some authors [18, 19, 23]. Plate-shaped metastable $NiSn_3$ phases grew faster at 130 °C than at 85 °C resulting in huge whiskers, just like those described by Chen and Chen [18]. The authors also reported Kirkendall voids along the $Ni_3Sn_4/NiSn_3$ interface as result of the Kirkendall effect. They assumed that the $NiSn_3$ IMC growth was only controlled by Ni. They also reported that their metastable $NiSn_3$ phase nucleated more slowly, but

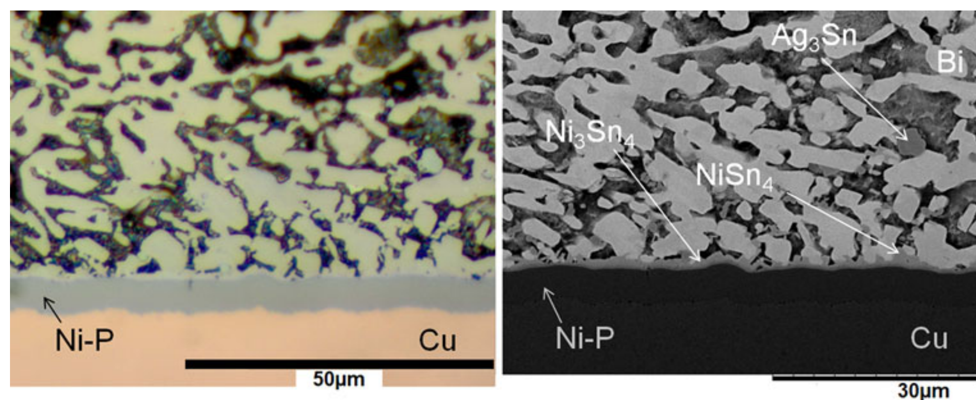

Fig. 2 Optical and SEM microscopy of the microstructure of Sn–57Bi–1Ag on ENIG aged at 85 °C for 800 h

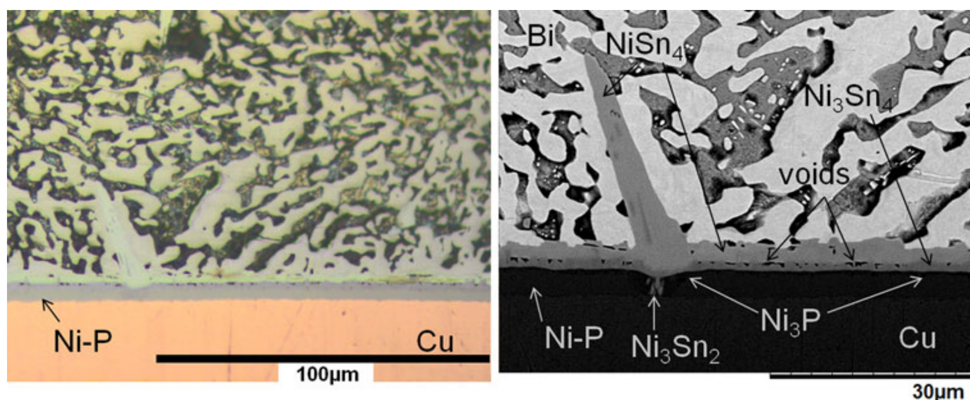

Fig. 3 Optical and SEM image of a sample aged at 130 °C annealed for 200 h

had a much faster growth rate than that of the Ni_3Sn_4 phase. In the next section, the growth rates of the Ni_3Sn_4 and $NiSn_4$ phase were calculated. After annealing at 100 °C at various times, Chen and Chen [18] neither found Ni_3Sn nor Ni_3Sn_2. In this study, a stoichiometry close to that of Ni_3Sn_2 was detected.

Solder/substrate IMC growth kinetics

To make quantitative predictions of the solder joint durability, it is indispensable to determine the growth kinetics. The faster the intermetallics of a solder/substrate couple grow at a given temperature, the more of the materials will be consumed. This can induce serious reliability problems to a solder joint. Therefore, quantitative measurements of the IMC layer growth under isothermal aging conditions are necessary to acquire the growth kinetics of a solder/substrate interconnect. For this purpose, the samples need to be stored under isothermal aging conditions while the temperature remains steady for a set time interval.

Since the growth process of solder/substrate interconnects can theoretically be suggested as diffusion controlled, the average layer thickness y can be plotted in a simply way against the square root of aging time $t^{0.5}$. The graphs for the IMC growth of Ni_3Sn_4 and $NiSn_4$ at 85 and 130 °C and their corresponding growth constants are given in Figs. 4 and 5. The high standard deviation in Fig. 5 represents the irregular $NiSn_4$ compound growth along the interface at 130 °C. The mathematical description results in the following simplified expression [7]:

$$y - y_0 = k \cdot t^{0.5}$$

where y_0 represents the initial layer thickness after reflow in m, and k the slope of thickness versus square root of aging time curve in m s$^{-0.5}$. Knowing the value of k at a particular temperature, the thickness of the IMC y as a function of time t can be calculated. k is called the growth

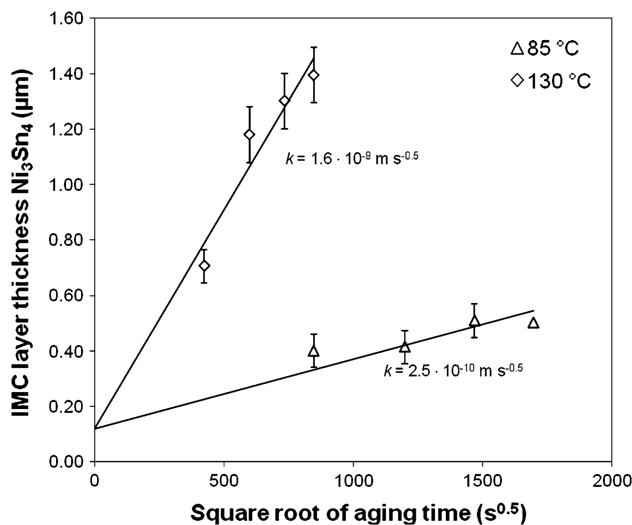

Fig. 4 IMC layer thickness of Ni_3Sn_4 versus square root of aging time for the temperatures 85 and 130 °C. The *error bars* represent the ±standard deviation of four measurements of each specimen

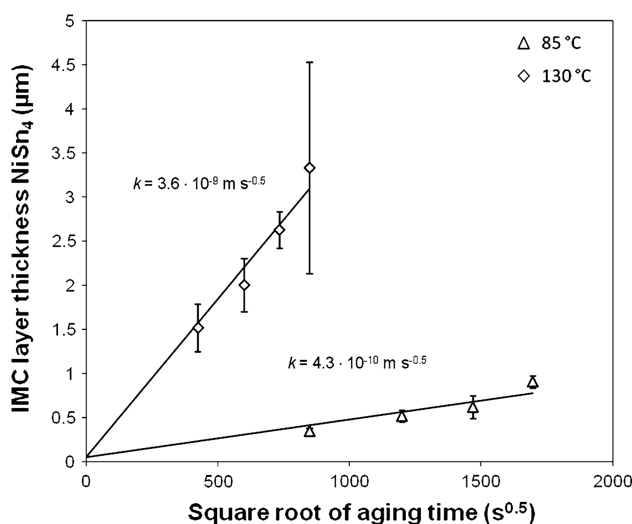

Fig. 5 IMC layer thickness of $NiSn_4$ versus square root of aging time for the temperatures 85 and 130 °C. The *error bars* represent the ±standard deviation of four measurements of each specimen

constant, including the activation energy ΔH in kJ mol^{-1}, the temperature T in K, and the universal gas constant $R = 8.314$ J mol^{-1} K^{-1} [7]. Now, an Arrhenius analysis can be performed that describes the layer growth with the following equation:

$$y - y_0 = A \cdot t^{0.5} \cdot \exp\left(-\frac{\Delta H}{RT}\right)$$

A represents the pre-exponential factor in m s$^{-0.5}$. If the growth constant k at different temperatures is known, assuming the growth mechanism will be the same at both temperatures, the activation energy ΔH can be determined. The slope of a plot $\ln(k)$ against the reciprocal of the absolute aging temperature $1/T$ indicates $\Delta H/R$. Figure 6 shows the graph with the corresponding activation energies ΔH for Ni_3Sn_4 and $NiSn_4$ of approximately 49 and 57 kJ mol^{-1}, respectively.

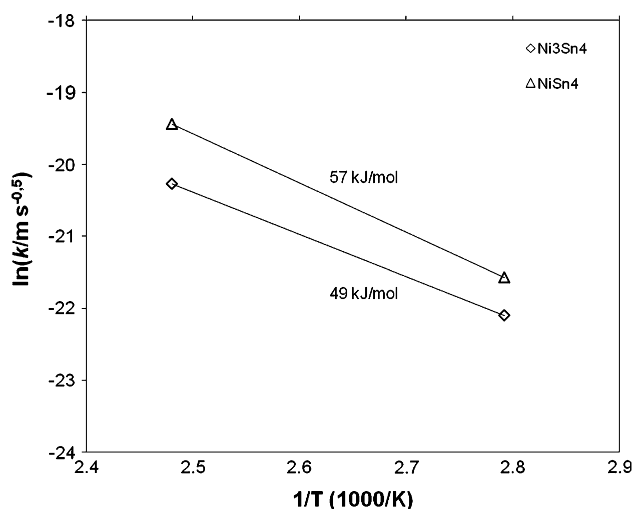

Fig. 6 The slope of a plot $\ln(k)$ against the reciprocal of the absolute aging temperature $1/T$ indicates $\Delta H/R$

Fracture behavior of the solder joint

As mentioned before, the growth of IMCs can influence the shear strength of a solder joint significantly. The brittleness of a Ni_3Sn_4 phase is well known. However, the shear strength of the solder joints does not only depend on the brittleness of the IMCs. It is further known that so called Kirkendall voids are also common failure mechanisms. Those voids, considered to be caused by the Kirkendall effect, were previously observed between the Ni-P layer and Sn-based solders [8]. The higher the density of those voids the lower the tensile strength. In this study, the influence of isothermal aging on the shear strength of a solder joint was analyzed. Shear strength measurements showed that the initial maximum shear strength of the solder joint rapidly decreased after solid-state thermal aging at 130 °C. Only 20% of its initial value remained after 100 h. The sheared ENIG/Sn–57Bi–1Ag/ENIG couple annealed at 130 °C for 100 h is shown in Fig. 7. In the optical micrograph, the crack is only visible at the interface. A closer inspection of the SEM micrograph shows a continuing spread of the crack along the $Ni_3Sn_4/NiSn_4$ interface. This indicates that the voids between the two phases assist the declining shear strength of the interconnection. This assumption can be made against the background that shear strength tests with samples stored at 85 °C showed less decline to about 86% of their initial values after 800 h. Furthermore, the void formation at 85 °C is rather small along the $Ni_3Sn_4/NiSn_4$ interface. Hence, the rapid shear strength loss of the Sn–57Bi–1Ag/Ni-P couple for high temperature applications has to be considered. For verification, further experiments are required.

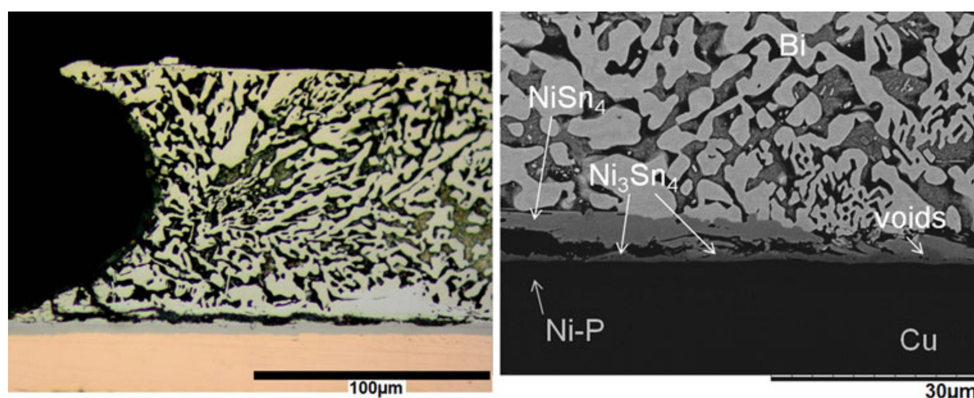

Fig. 7 Optical and SEM micrograph of a sheared ENIG/Sn–57Bi–1Ag/ENIG couple after annealing at 130 °C for 100 h

Conclusions

This article summarizes metallographic analyses of Sn–57Bi–1Ag/ENIG couples after isothermal aging at 85 and 130 °C. The intermetallics were determined by EDX analyses. At the interface, the two intermetallics Ni_3Sn_4 and $NiSn_4$ coexisted in the diffusion couples stored at 85 and 130 °C. The Ag_3Sn IMC distributed inside the microstructure.

Furthermore, the interfacial growth kinetics as a result of this isothermal aging process was investigated. Both intermetallics, Ni_3Sn_4 and $NiSn_4$, grew rather slowly at 85 °C, with their corresponding growth constants k at 2.5×10^{-10} and 4.3×10^{-10} m $s^{-0.5}$, respectively. At 130 °C, their growth constants k were at 1.6×10^{-9} and 3.6×10^{-9} m $s^{-0.5}$. After 200 h, Ni_3Sn_4 and $NiSn_4$ reached an average thickness of 1.4 and 3.3 µm, respectively. With this data, the activation energy ΔH for both intermetallics could be approximated. The calculated activation energy was 49 kJ mol^{-1} for Ni_3Sn_4 and 57 kJ mol^{-1} for $NiSn_4$.

Moreover, this rapid $NiSn_4$ phase growth at high isothermal temperatures resulted in the generation of Kirkendall voids between the Ni_3Sn_4/$NiSn_4$ interface. A high density of those voids decreased the maximum shear strength of the solder joint significantly. This can result in reliability problems of electronic devices. When using Sn–57Bi–1Ag solder on ENIG substrate, this should be taken into account as early as in the design process.

References

1. Chen SW, Wang CH, Lin SK, Chiu CN (2007) In: Subramanian K (ed) Lead-free electronic solders: a special issue of journal of materials science: materials in electronics, 1st edn. Springer, New York, p 19
2. Abtew M, Selvaduray G (2000) Mater Sci Eng 27(5/6):95
3. Kang SK, Sarkhel AK (1994) JEM 23(8):701
4. Suganuma K (2002) ESPEC Technol Rep 13:1
5. Hwang JS (2001) Environment-friendly electronics: lead-free technology. Electrochemical Publications, Isle of Man
6. Dong W, Shi Y, Zhidong Xia, Lei Y, Guo F (2008) J Electron Mater 37(7):982
7. Vianco PT (1999) Soldering handbook, 3rd edn. American Welding Society, Miami
8. Shangguan D (2005) Lead-free solder interconnect reliability. ASM International, Materials Park
9. Frear DR (2007) In: Subramanian K (ed) Lead-free electronic solders: a special issue of journal of materials science: materials in electronics, 1st edn. Springer, New York, p 319
10. Vianco PT, Kilgo AC, Grant R (1995) J Electron Mater 24(10):1493
11. Liu Z, Shang P, Pang X, Shang J (2008) In: IEEE ICEPT-HDP
12. Kang T, Xiub Y, Liu C, Hui L, Wang J, Tonga W (2011) J Alloy Compd 509(5):1785
13. Chen C, Ho CE, Lin AH, Luo GL, Kao CR (2000) J Electron Mater 29(10):1200
14. Yoon J, Lee C, Jung S (2002) Mater Trans 43(8):1821
15. Young B, Duh J (2001) J Electron Mater 30(7):878
16. Wang J, Liu HS, Liu LB, Jin ZP (2006) J Electron Mater 35(10):1842
17. Haimovich J (1989) Weld J 68(3):102
18. Chen C, Chen S (2003) J Mater Res 18(6):1293
19. Boettinger WJ, Vaudin MD, Williams ME, Bendersky LA, Wagner WR (2003) J Electron Mater 32(6):511
20. Chuang HY, Chen WM, Shih WL, Lai YS, Kao CR (2011) In: Electronic Components and Technology Conference, p 1723
21. Glazer J (1994) J Electron Mater 23(8):693
22. Kattner UR, Boettinger WJ (1994) J Electron Mater 23(7):603
23. Wang C, Kuo C, Chen H, Chen S (2011) Intermetallics 19(1):75